Available online at www.sciencedirect.com
ScienceDirect
Surface Science 602 (2008) 1020–1031
SURFACE SCIENCE
www.elsevier.com/locate/susc

A reactive force field (ReaxFF) for zinc oxide

David Raymand [a], Adri C.T. van Duin [b], Micael Baudin [a], Kersti Hermansson [a,*]

[a] Department of Materials Chemistry, The Ångström Laboratory, Box 538, S-75121 Uppsala, Sweden
[b] Materials and Process Simulation Center (MSC), California Institute of Technology, Pasadena, CA 91125, USA

Received 28 August 2007; accepted for publication 13 December 2007
Available online 28 December 2007

Abstract

We have developed a reactive force field (FF) within the ReaxFF framework, for use in molecular dynamics (MD) simulations to investigate structures and reaction dynamics for ZnO catalysts. The force field parameters were fitted to a training set of data points (energies, geometries, charges) derived from quantum-mechanical (QM) calculations. The data points were chosen to give adequate descriptions of (the equations of state for) a number of zinc metal and zinc oxide phases, a number of low-index ZnO surfaces and gas-phase zinc hydroxide clusters. Special emphasis was put on obtaining a good surface description. We have applied the force field to the calculation of atomic vibrational mean square amplitudes for bulk wurtzite–ZnO at 20 K, 300 K and 600 K and we find good agreement with experimental values from the literature. The force field was also applied in a study of the surface growth mechanism for the wurtzite(0 0 0 1) surface. We find that the growth behavior depends on the presence of surface steps.

Keywords: Zinc oxide; Construction and use of effective interatomic interactions; Molecular dynamics; Density-functional calculations; Surface relaxation and reconstruction; Surface energy

1. Introduction

The aim of this study is to create a high-level, transferable interaction model for the condensed phases of zinc oxide. ZnO is a highly interesting material with a broad range of technical applications. It is known to catalyze a number of chemical reactions, such as the decomposition of formic acid and the formation of methanol from CO and H_2 [1–3]. Recent studies of ZnO nanostructures imply a connection between catalytic activity and surface morphology [1]. ZnO also attracts interest because of its electronic properties, with a semi-conducting band-gap of 3.4 eV. It has potential applications in opto-electronic devices, directly or as a substrate for the growth of other semiconductors such as GaN and SiC; here the interest in ZnO is partly fueled by the availability of high-quality substrates [4].

Because of this large versatility of ZnO, it is not surprising that a very large number of both experimental and theoretical studies of ZnO exist in the literature. Thus, for the various polymorphs of bulk ZnO only, numerous theoretical studies have been published, using models based either on quantum-mechanical (QM) methods (*ab initio* theory or density-functional theory (DFT)) or analytical force fields (FF). Some recent examples of such QM studies can be found in Refs. [5–7] (and references therein). In Ref. [5], Catti et al. studied the piezo-electric properties of ZnO using Hartree–Fock calculations, and in Refs. [6,7], the optimized geometry and electronic structure as well as the effect of pressure on the vibrations in several ZnO polymorphs were studied using DFT lattice dynamics.

The development of DFT techniques, or hybrid techniques such as the B3LYP functional [8,9], have resulted in methods that are significantly more efficient than *ab initio* methods of comparable accuracy. However, no

* Corresponding author. Tel.: +46 18 47 137 67; fax: +46 18 513 548.
E-mail address: kersti@mkem.uu.se (K. Hermansson).

0039-6028/$ - see front matter © 2007 Elsevier B.V. All rights reserved.
doi:10.1016/j.susc.2007.12.023

DFT method available today is fast enough to describe chemical and physical properties accurately in large, dynamic systems with a few thousand atoms. Many systems with defects of various kinds and broken symmetries would ideally require such large systems. Therefore force field based methods are necessary.

ZnO is challenging to model by means of force field methods because of its partly covalent, partly ionic character. Traditionally, metal oxides have been modeled successfully using pair interactions consisting of a short-range part and long-range Coulombic terms, the latter usually modeled by fixing the charges of the different ions at their formal values. Such a procedure of course limits the possibility to describe a charge redistribution around a defect or at a surface. By adding an extra (charged) site to each ion connected via a spring, polarization can be handled; this is the idea behind the shell-model, [10] which can thus capture some of the many-body interactions, even in an otherwise pair-additive model. The short-range interactions in the shell-model are usually described by an analytical expression such as the Buckingham interaction model. Several successful attempts at using these schemes for ZnO can be found in Refs. [11–14]. In Ref. [11], a shell-model potential was used to predict the spatial arrangement of the dopant species sodium, lithium, and chlorine within the zinc oxide lattice in varistors using molecular dynamics (MD) simulations. The shell-model of Ref. [11] was also applied in the MD study of elastic properties of zinc oxide "nanobelts" in Ref. [14]. Whitmore et al. [12] used lattice dynamics calculations to parametrize a shell-model reproducing bulk vibrational properties of ZnO. This model has subsequently been applied to embed QM-clusters [13] in the investigation of electron trapping at the oxygen terminated polar (0001) surface of ZnO and related surface F centers.

The pure two-body potentials as well as the various shell models generally have difficulties in describing the covalent character of ZnO properly, as is evident from the fact that the four-coordinated wurtzite does not come out as the lowest-energy crystal structure in Refs. [11,12]. Instead, these models tend to favor the more isotropic, four-coordinated zincblende (sphalerite) structure. The description of covalent bonding can be aided by the use of explicit higher-order terms in the many-body expansion. One such example of the addition of a three-body interaction term can be found in the MD study of the growth mechanism for the ZnO(0001) surface in Ref. [15]. Another way to handle the covalent character of ZnO has been to neglect the ionic character altogether and use a *bond-order potential*, i.e. a potential where the short-range many-body effects depend on the local environment of each atom (the number of neighbors and the distances to them). This has recently been done in a successful way by Erhart et al. [16]. Such an approach might, however, have difficulties in modeling interfaces, or in other cases where Coulombic fields might be important. Moreover, if only nearest neighbors are considered, the model cannot describe the energy difference between the two four-coordinated ZnO phases. Incidentally, Ref. [16] gives an excellent review of different analytical potential schemes used for ZnO in the literature. In the present study, we will use the reactive force field (ReaxFF) framework to model ZnO.

The ReaxFF model [17–19] is also a bond-order interaction model. It is bond-order consistent for the two-body, three-body and four-body short-range interaction terms. The model also includes Coulombic terms, where the charges are calculated based on connectivity and geometry using the Electronegativity Equalization Method (EEM) [20], thereby allowing redistribution of charges. In principle these features allow the ReaxFF model to describe metallic, covalent and ionic bonds. The ReaxFF model is able to simulate the breaking and reforming phenomena of bonds during dynamics. It can also reproduce the structures and mechanical properties of condensed phases [17–19]. The ReaxFF framework was initially developed for hydrocarbons [17,18], and has since then been applied to many such systems. It has also been employed in the study of several oxide systems, namely MoO_x, V_xO_y and Bi_xO_y [21] oxides and Si/SiO_2 [18] and Al/Al_2O_3 [19] oxide interfaces.

All force field parameters within the ReaxFF framework are developed using results of quantum-chemical calculations. During the parametrization, measures are taken to provide for transferability, e.g. the parameters describing the oxygen–oxygen interaction are the same in all compounds and molecules. Therefore the set of data points to which the model is fitted needs to contain information about a wide range of compounds. In the current study this means having data not only for ZnO(s) and its surfaces, but also for Zn(s) and Zn and O containing gas-phase species. The ZnO parameters may thus in principle be used not only for the metal oxide but also for the metal/oxide interface and for systems where Zn or ZnO interact/react with hydrogen, hydrocarbons, and other interesting molecules (provided that a parametrization for the molecule is available and that the ZnO molecule cross-terms can be made).

However, parameterizing a model for a broad range of chemical environments might necessitate trade-offs. To ensure a good description of the most important parts of the data set, a weighting scheme is employed during the parametrization. In our case describing ZnO(s) and its surfaces were prioritized over the description of gas-phase hydroxide clusters. If future studies require greater accuracy for the gas-phase species, the weighting scheme could be redesigned to allow a closer reproduction of these data points.

The current parametrization of ZnO in the ReaxFF model consisted of the following steps: (i) The creation of an initial training set of data points (energies, charges and geometries) from QM calculations, (ii) selection of the appropriate number of terms in the ReaxFF energy expression, (iii) fitting the parameters to the training set, (iv) evaluating if the data set is satisfactorily reproduced or if the energy expression needs to be expanded with addi-

tional terms which may in turn require the training set to be expanded with additional data points, (v) repeating (i)–(iv) until the fit is satisfactory, and (vi) validation of the potential parameters by comparing properties extracted from the model to experimental and quantum-chemical data from other studies.

The layout of the paper is as follows. Section 2 describes the methods used, and gives information about the ReaxFF model (Section 2.1), the force field optimization procedure (Section 2.2) and the quantum-mechanical calculations used to generate the data set (Section 2.3). Section 3 is the results and discussion section, where we present the model and make an assessment of its quality by discussing the model's ability to reproduce the relative energies for the different crystalline phases and for certain low-index surfaces. In Section 4, we apply the new model in MD simulations to calculate the vibrational mean square amplitudes (or displacements) of the atoms in bulk wurtzite ZnO and to study wurtzite ZnO(0 0 0 1) surface growth. In the growth simulations we use a strategy as similar as possible to the published force field study of Kubo et al. [15] and compare with their results. The paper ends with a summary section.

2. Method

Zinc oxide is a transition metal oxide with the wurtzite type structure (space group $P6_3mc$; number 186 in *the International tables for crystallography* [22]) with lattice constants 3.24992(5) and 5.20658(8) Å at ambient conditions [23]. It has a bulk modulus of 140 GPa [24]. Another three polymorphs discussed in the literature are listed in Table 1 together with experimental cell parameters and bulk moduli, where such data exist. Calculated data in the table will be discussed in Sections 2.3 (B3LYP) and 3 (ReaxFF).

2.1. The reactive force field

The total interaction energy expression of the ReaxFF is partitioned into several energy terms as given in Eq. (1).

$$E_{\text{system}} = E_{\text{bond}} + E_{\text{over}} + E_{\text{under}} + E_{\text{lp}} + E_{\text{val}} + E_{\text{pen}} + E_{\text{tors}} + E_{\text{conj}} + E_{\text{vdWaals}} + E_{\text{Coulomb}}. \quad (1)$$

These partial contributions include bond energies (E_{bond}), under-coordination penalty energies (E_{under}), lone-pairs energies (E_{lp}), over-coordination penalty energies (E_{over}), valence angles energies (E_{val}), energy penalty for handling atoms with two double bonds (E_{pen}), torsion angles energies (E_{tors}), conjugated bonds energies (E_{conj}) and terms to handle non-bonded interactions, namely van der Waals (E_{vdWaals}) and Coulomb (E_{Coulomb}) interactions. All terms except the last two are bond-order dependent, i.e. will contribute more or less depending on the local environment of each atom.

In the expression above, E_{vdWaals} and E_{Coulomb} are calculated between *every* atom pair, irrespective of connectivity and include a shielding parameter to avoid excessive repulsion at short distances. This treatment of non-bonded interactions aids the ReaxFF model in describing covalent, metallic, ionic, and intermediate materials and thus greatly enhances its transferability. A detailed description of the individual terms can be found in Refs. [17,18].

In the present study, not all of the terms in Eq. (1) were considered necessary and some were therefore set to zero, reducing the energy expression to Eq. (2).

$$E_{\text{system}} = E_{\text{bond}} + E_{\text{over}} + E_{\text{val}} + E_{\text{vdWaals}} + E_{\text{Coulomb}}. \quad (2)$$

Table 1
QM results and ReaxFF results (at 0 K) compared to experimental data from the literature (at room temperature) for the cell axes, heats of formation ($\Delta_f H$), bulk moduli and elastic constants of the four polymorphs (B1–B4) of ZnO

Structure	Property	B3LYP	ReaxFF	Experiment
Wurtzite(B4)	a/Å	3.28[a]	3.29	3.25 [23]
$P6_3mc$	c/Å	5.28[a]	5.30	5.21 [23]
	$\Delta_f H_{B4}$/(kcal/mol)		−91.2	−83.3[a] [37]
	Bulk modulus/GPa	136	144	141, 143 [24,44]
	c_{11}/GPa		222.9	209.7 [45]
	c_{12}/GPa		116.3	121.1 [45]
	c_{13}/GPa		103.5	105.1 [45]
	c_{33}/GPa		212.8	210.9 [45]
	c_{44}/GPa		57.1	42.47 [45]
Zincblende(B1)	Bulk modulus/GPa	162	130	Polymorph does not occur in nature
$F\bar{4}3m$	a/Å	4.60[a]	4.62	
	$\Delta_f H_{B1} - \Delta_f H_{B4}$/(kcal/mol)	0.50[a]	0.97	
Rocksalt(B3)	Bulk modulus/GPa	202	283	203,228 [44,46]
$Fm\bar{3}m$	a/Å	4.30[a]	4.44	4.27 [46]
	$\Delta_f H_{B3} - \Delta_f H_{B4}$/(kcal/mol)	8.57[a]	7.72	
Caesium chloride(B2)	Bulk modulus/GPa	183	407	Polymorph does not occur in nature
$Pm\bar{3}m$	a/Å	2.68[a]	2.64	
	$\Delta_f H_{B2} - \Delta_f H_{B4}$/(kcal/mol)	37.89[a]	37.58	

[a] Explicitly entered in the dataset.

2.2. Force field optimization procedure

The ReaxFF for ZnO was optimized using a successive one-parameter search technique as described by van Duin et al. [25]. Based on QM calculations for Zn(s), ZnO(s) and Zn hydroxide clusters, ReaxFF parameters were generated for Zn–O and Zn–Zn bond energies and for Zn–O–Zn, O–Zn–O, O–Zn–Zn and Zn–O–H valence angle energies.

The current parametrization of ZnO in the ReaxFF model consisted of the following steps, as outlined in the introduction (the same roman numerals are used).

(i) An initial training set of QM data points was created for clusters and crystals. For the crystals, data for the energy dependence on volume of four Zn metal phases and four ZnO polymorphs were included: Wurtzite(4), zincblende(4), rocksalt(6) and caesium chloride(8) for ZnO and fcc(12), hcp(12), bcc(8) and sc(6) metal phases (coordination number in parenthesis). Mulliken charges for the ZnO bulk systems were added to the dataset. A bond dissociation profile of one Zn–OH bond in a $Zn(OH)_2$-molecule was included. Data for the energy dependence on valence angles in $Zn(OH)_2$ and $O(ZnOH)_2$ was added to include valence angle variation in clusters. The ReaxFF parameters were fitted to the lowest-energy state (singlet or triplet depending on geometry).

(ii) A minimum number of terms in the ReaxFF energy expression were selected (starting with $E_{\text{bond}}, E_{\text{over}}, E_{\text{vdWaals}}, E_{\text{Coulomb}}$).

(iii) The parameters were fitted to the whole training set using the built-in one-parameter routine.

(iv)–(v) The valence angle term (E_{val}) was added to the total energy expression to obtain a good fit to the training set. Surface energies and geometries for certain low-index surfaces of three of the ZnO(s) phases were added to improve the description of ZnO surfaces. These surfaces were wurtzite $(10\bar{1}0)$ and $(11\bar{2}0)$, zincblende (100), rocksalt (110) and (100). To further expand the data set, Mulliken charges from the surface calculations were added.

(vi) The potential parameters were validated by comparing properties extracted from the model to experimental and quantum-chemical data; see Section 3.

In total 44 parameters were fitted to a dataset containing 347 data points.

2.3. The quantum-mechanical calculations and the systems studied

The quantum-mechanical calculations were performed with the GAUSSIAN03 program [26] for the hydroxide clusters and the CRYSTAL03 program [27] for the ZnO crystals and surface systems. The calculations for Zinc metal were performed with the SeqQuest software package [28].

2.3.1. System descriptions

QM calculations were performed for the four *crystal polymorphs* of the wurtzite, zincblende, rocksalt and caesium chloride structures (the structures are also referred to as h-ZnS, c-ZnS, NaCl and CsCl, respectively). Here 3D periodic calculations were performed using the CRYSTAL03 program [27], which makes use of space group symmetry. For a range of volumes, the cell parameters of the four crystal structures were optimized within the given space groups in such a way that the minimum energy for a given volume was obtained (e.g. the c/a-ratio was optimized for the wurtzite structure). Potential energy curves were calculated for use in the training set for the ReaxFF parametrization. The bulk moduli were calculated using the Murnaghan equation; see Ref. [24] a for detailed description of the procedure for ZnO. The bulk moduli were used for ReaxFF model validation purposes (and were not included in the training set). The elastic constants of the wurtzite phase were calculated following the procedure outlined in Ref. [29].

Five ZnO *surface systems* were studied, namely $(10\bar{1}0)$ and $(11\bar{2}0)$ for wurtzite, (110) for zincblende and (110) and (100) for the rocksalt structure. Each surface system was modeled by an isolated slab, periodic in two dimensions (x and y), with free surfaces in the third ($+z$ and $-z$). In all cases, 10-layer slabs were generated by the built-in routine of CRYSTAL03, thus preserving symmetry operations of the space group where possible. The number of layers was chosen based on the slab-thickness investigation for wurtzite by Wander and Harrison [30]. The periodic cell axes of the slabs were kept fixed at the respective optimized bulk values (see Table 1). The atomic positions were optimized for all slabs (with fixed cell parameters).

The surface energy (defined as $(E_{\text{surf}} - nE_{\text{bulk}})/2A_{\text{surf}}$, where A_{surf} is the surface area and n is the number of ZnO formula units in the slab cell), the surface relaxation (defined as the atomic displacements in the z-coordinate) and the surface rumpling (defined as the difference in relaxation between the cations and the anions in one layer, positive rumpling meaning that the cations displace more towards the center of the slab compared to the anions) were calculated and used in the training set.

Equations of state were calculated for four polymorphs of *zinc metal*: hexagonally close packed (hcp), face centered cubic (fcc), body centered cubic (bcc) and simple cubic (sc). Here 3D periodic calculations were performed using the SeqQuest program [28]. The cell parameters of the three crystal structures were optimized within the given space groups, following the same procedure as for the ZnO crystals. Potential energy curves were calculated for use in the training set for the ReaxFF parametrization.

Geometry optimizations and potential energy curve calculations were performed for the two *zinc hydroxide*

Table 2
The final atom parameters for Zn

		Coulomb parameters				van der Waals parameters			
	r_0	η (eV)	χ (eV)	γ (Å)	$p_{ov/un}$	r_{vdW} (Å)	ϵ (kcal/mol)	α	γ_{vdW}(Å)
Zn	1.9014	5.6773	0.5149	0.8009	−2.5000	1.9272	0.3000	11.4526	12.5107
O	1.2477	8.9989	8.5000	1.0503	−3.6141	1.9236	0.0904	10.2127	7.7719

For O, parameters from Ref. [49] was used. Definitions of the individual ReaxFF parameters in this table and Tables 3–5 can be found in Refs. [17,18].

clusters, $Zn(OH)_2$ and $O(ZnOH)_2$, using the GAUSSIAN03 program [26].

2.3.2. Computational details

All calculations for the *ZnO crystals and surfaces* were performed using 3- and 2-dimensionally periodic systems (as mentioned) and the hybrid DFT functional B3LYP. Gaussian type basis sets were used for both the zinc atom and the oxygen atom, as optimized by Jaffe and Hess [24]. This basis set has been applied with good results in several earlier QM-studies of ZnO polymorphs and surfaces [30–32]. In the 3-dimensionally periodic calculations, the Brillouin zone was sampled with a $10 \times 10 \times 10$ *k*-point sampling mesh of the Monkhorst–Pack type [33]. In the 2-dimensionally periodic calculations, the Brillouin zone was sampled with 4×4 *k*-point sampling mesh of the Monkhorst–Pack type. Table 1 gives a comparison of the optimized QM results with experiment for ZnO.

The calculations for the *zinc metal* were performed using 3-dimensionally periodic systems and the DFT functional PBE [34]. A library SeqQuest atom file for Zn was used, describing a gaussian type basis set with double zeta quality for s and d plus polarization for p. The atom file includes a pseudo potential generated using the Fritz–Haber Institute *fhi98PP* code [35]. However, the wave function coefficients in the SeqQuest atom file were optimized to get good Zn cell parameters and energies. The Brillouin zone was sampled with a $8 \times 8 \times 8$ *k*-point sampling mesh. Table 2 gives a comparison of the optimized QM results with experiment for Zn. The experimental cohesive energy for Zn was used in the training set [36].

The zinc metal data and ZnO crystal data were combined in the training set by putting the energies on a heat of formation scale, using the experimental heat of formation [37].

For the *clusters*, potential energy curves were calculated as functions of the HOZn–OH bond distance and the HO–Zn–OH, Zn–O–H and (HOZn)–O–(ZnOH) valence angles, using the hybrid DFT functional B3LYP [8,9] and the 6-311 + G^* basis set [38–40] as implemented in the GAUSSIAN03 program.

3. Results and discussion

Our final fitted ReaxFF for ZnO is given in Tables 2–5. The potential form was given schematically in Eq. (2). Unless otherwise stated, all ReaxFF results in the following text, tables or figures refer to our final optimized ReaxFF,

Table 3
The final van der Waals and bond radius parameters for the Zn–O bond

Bond	r^{σ} (Å)	r_{vdW} (Å)	ϵ (kcal/mol)	γ_{vdW} (Å)
Zn–O	2.0933	2.1496	0.2992	9.7788

Table 4
The final bond energy and bond-order parameters for the Zn–Zn and Zn–O bonds

	D_e^{σ}/(kcal/mol)	$p_{be,1}$	$p_{be,2}$	$p_{bo,1}$	$p_{bo,2}$	p_{kov}
Zn–Zn	47.2436	−0.3583	2.7689	0.0962	6.3816	0.0000
Zn–O	124.8335	−0.8979	1.1391	−0.3406	6.7964	0.0000
O–O	60.1436	−0.2802	0.2441	−0.1302	6.2919	0.9114

The O–O parameters from Ref. [49] were used.

Table 5
The final valence angle parameters

Valence angle	$\Theta_{0,0}$ (degree)	k_a (kcal/mol)	k_b $(1/\text{rad})^2$	$p_{v,1}$	$p_{v,2}$
H–O–Zn	50.7176	11.0788	0.3108	0.9582	1.1056
O–Zn–O	9.4094	26.4927	0.3247	2.0000	3.1031
Zn–O–Zn	50.1486	6.7868	0.5367	0.1384	1.1000
O–Zn–Zn	64.3179	6.5137	0.2554	0.5219	1.7398

also when we discuss selected cuts through the multi-dimensional potential energy surface (PESs), such as bond dissociation curves, etc., below. The quantities included in the final FF fit were listed in Section 2.2. In the figures presented in the following, selected cuts through, or points on, the final ReaxFF PESs will be compared with the corresponding cuts from the B3LYP PESs.

3.1. Equations of state for the Zn and ZnO crystals

As mentioned, the relative stabilities of four Zn crystal structures (fcc, hcp, bcc and sc types) and four ZnO crystal structures (wurtzite, zincblende, rocksalt and caesium chloride) were used as data in the ReaxFF training set. The variation of coordination numbers and coordination figures represented in these crystals give important information concerning how bond energies and valence angles energies relate to bond order. The heats of formation and cohesive energies for the various crystals were used in the training set and give information about bond strength as a function of bond order. In this study, we find that the inclusion of the valence angle term has a large influence on the relative phase stability of the crystals. The cell axis lengths of the different crystals give important information

about the positions of the minima of the bond dissociation profiles. No information about the elastic properties of the crystals was entered in the data set other than the volume-energy relationship (equations of state). Therefore calculating elastic constants and bulk moduli of the crystal structures may serve to evaluate the parametrization, which has been done here and is presented below. During the force field optimization, the description of the crystal phases was given priority over the clusters, since the crystals were considered more important for future studies (see below).

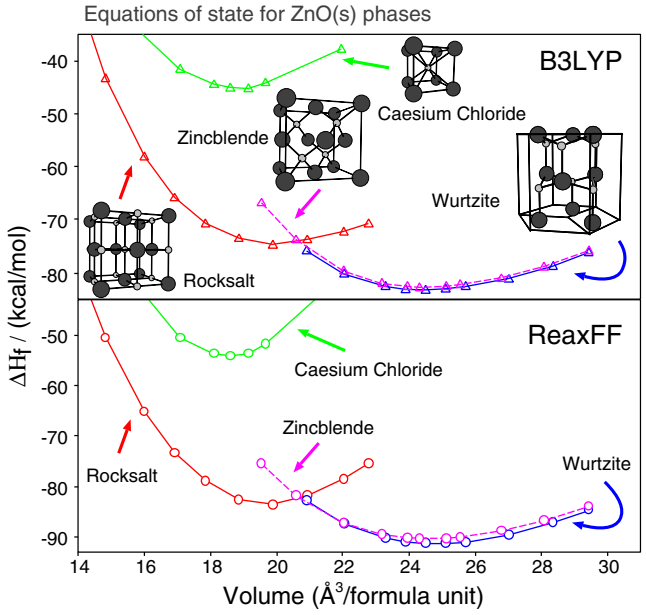

Fig. 1. Equation of state (compression and expansion) for four crystal structures (wurtzite(B4), zincblende(B3), caesium chloride(B2) and rock-salt(B1)) of ZnO calculated using the (a) B3LYP and (b) ReaxFF methods.

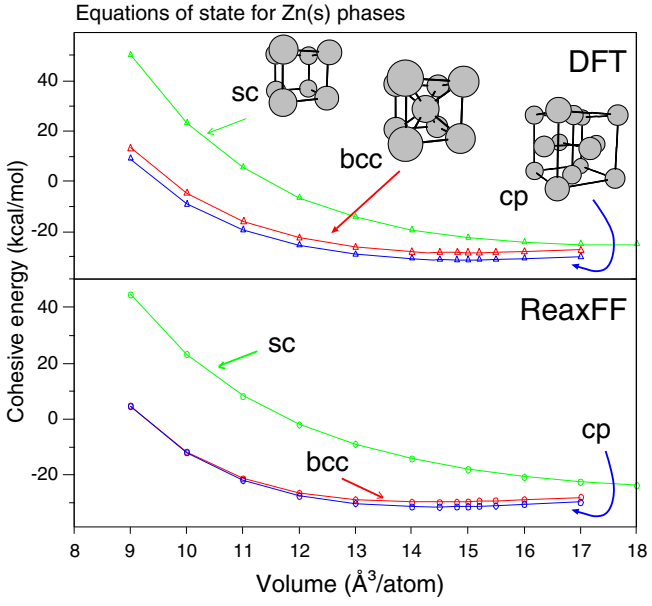

Fig. 2. Equation of state (compression and expansion) for three crystal structures (simple cubic (sc), body centered cubic (bcc) and close-packed (cp)) of Zn calculated using the (a) PBE and (b) ReaxFF methods.

Fig. 1 shows that the four ZnO polymorphs are reproduced in the correct relative order of stability by the ReaxFF model, and also the curve shapes agree with the QM data. It is known from the literature that ReaxFF has a systematic tendency to overestimate the stability of metal oxide phases; [21] this is also the case here. Table 1 gives a comparison between bulk moduli and cell axes of the various polymorphs of ZnO obtained with the B3LYP method, the ReaxFF model and experiment, respectively. We find that the ReaxFF model gives a good description of the elastic properties of wurtzite structured ZnO(s) compared to experimental values. This helps validate the quality of the current parametrization since information about the elastic properties of the crystals was only implicitly entered. A good description of the low-energy wurtzite phase was prioritized in our fitting; this is visible from the overestimation of the bulk moduli of the high-energy phases.

Fig. 2 shows the equations of state for zinc metal. Valence angle terms for pure Zn metal–metal interactions were not included; therefore the ReaxFF model will

Table 6
QM results and ReaxFF results (at 0 K) compared to experimental data from the literature (at room temperature) for the cell axes, cohesive energies, bulk moduli and elastic constants of Zn metal

Structure	Property	PBE	ReaxFF	Experiment
hcp	a/Å	2.63[a]	2.73[b]	2.67 [47]
$P6_3/mmc$	c/Å	5.06[a]	4.46[b]	4.95 [47]
	$E_{cohesive}$(hcp)/(kcal/mol)		−31.6	−31.1[a] [36]
	Bulk modulus/GPa	66.7	87.7	64.5–75.1[c]
	c_{11}/GPa		193	163[c]
	c_{12}/GPa		41	31[c]
	c_{13}/GPa		42	48[c]
	c_{33}/GPa		188[d]	60[c]
	c_{44}/GPa		71[d]	39[c]
fcc	Bulk modulus/GPa	81.8	87.7	Polymorph
$F\bar{4}3m$	a/Å	3.86[a]	3.86	does
	$E_{cohesive}$(fcc)-$E_{cohesive}$(hcp)/(kcal/mol)	1.31	0.00[b]	not occur in nature
bcc	Bulk modulus/GPa	84.6	73.5	Polymorph
$Im\bar{3}m$	a/Å	3.06[a]	3.06	does
	$E_{cohesive}$(bcc)-$E_{cohesive}$(hcp)/(kcal/mol)	2.71	2.71	not occur in nature
sc	Bulk modulus/GPa	64.2	30.2	Polymorph
$Pm\bar{3}m$	a/Å	2.71[a]	2.71	does
	$E_{cohesive}$(sc)-$E_{cohesive}$(hcp)/(kcal/mol)	6.00	6.62	not occur in nature

[a] Explicitly entered in the dataset.
[b] Valence angle terms for pure Zn were not included in the ReaxFF energy expression; therefore ReaxFF will preserve the ideal c/a ratio ($(8/3)^{1/2}$) of a close packed crystal. Also the volume vs. energy relationship for the fcc and hcp phases will be identical.
[c] Experimental values taken from the review article by Ledbetter [48].
[d] These hcp-specific stresses are not correctly reproduced for the reason stated in b.

preserve the ideal c/a ratio ($(8/3)^{1/2}$) of a close-packed crystal (i.e. there will be no energy difference between hcp and fcc). This also means that the hcp-specific elastic constants, i.e. c_{33} and c_{44}, corresponding to stresses in the c-direction of the hexagonal lattice, may not be correctly described. However, these valence angle terms can be added to the model at a later time if one wants to study properties relying on the elastic properties of hcp-Zinc. In the current study this feature has not been prioritized. Table 6 gives a comparison between bulk moduli and cell axes of the various Zn metal polymorphs calculated with the PBE method and the ReaxFF model and from experiment.

3.2. ZnO surfaces – energies and geometries

The surface structures of five different ZnO slabs were fitted. The correct relative order of the surface energies is important for studies of e.g. crystal growth, where high surface-energy facets tend to grow the fastest. Only non-polar surfaces were used in the training set because of the inherent difficulties of making a good QM-model of polar surfaces. Table 7 compares the surface energies from QM and ReaxFF. Reproducing the correct rumpling trends is important for a proper description of surface chemistry, and in our ReaxFF fitting, efforts were therefore made to reproduce the rumpling trends observed in the B3LYP calculations. Several inter-ionic distances in the slabs were added explicitly to the training set, to put extra weight on the surface geometry.

Table 7
QM results versus ReaxFF model results for surface energies of the five ZnO surfaces present in the ReaxFF training set

	B3LYP surface energy/Jm^{-2}	ReaxFF surface energy/Jm^{-2}
Wurtzite(10$\bar{1}$0)	1.32	0.96
Wurtzite(11$\bar{2}$0)	1.39	1.06
Zincblende(100)	1.30	1.00
Rocksalt(100)	1.16	0.73
Rocksalt(110)	2.00	1.10

Fig. 3 shows that ReaxFF tends to underestimate the surface relaxation (this underestimation is also visible in the surface energies) but reproduces the relative magnitudes of the relaxation of the different surface orientations compared to the QM-data.

3.3. Atomic charges in ZnO bulk and slabs

Since the EEM-method uses geometry and connectivity to calculate the magnitude of the ionic charges it is important to include such QM data in the training set. Therefore the charges of the ions in the ZnO bulk crystals and slabs were included in the training set. The coordination of the ions changes from the surface to the bulk of the slab and so do the charges. Here Mulliken charges were used to remain consistent with previous parameterizations in the ReaxFF model. Atomic charges in the four bulk crystal structures (Table 8) and the five slabs (Fig. 4) were fitted. In the slabs, the ReaxFF charge dependence on z-coordinate is seen to be slightly exaggerated compared to the B3LYP results. Likewise in the bulk ZnO crystals, the charge difference between ions with different coordination numbers is seen to be slightly exaggerated. Overall, the ReaxFF gives a good representation of the partial atomic charges of zinc and oxygen.

3.4. Potential energy curves for zinc hydroxide clusters

In line with the ReaxFF strategy of parametrization, we have also included data for selected zinc and oxygen containing gas-phase clusters. To include cluster data for the Zn–O bond, a dissociation profile was determined from

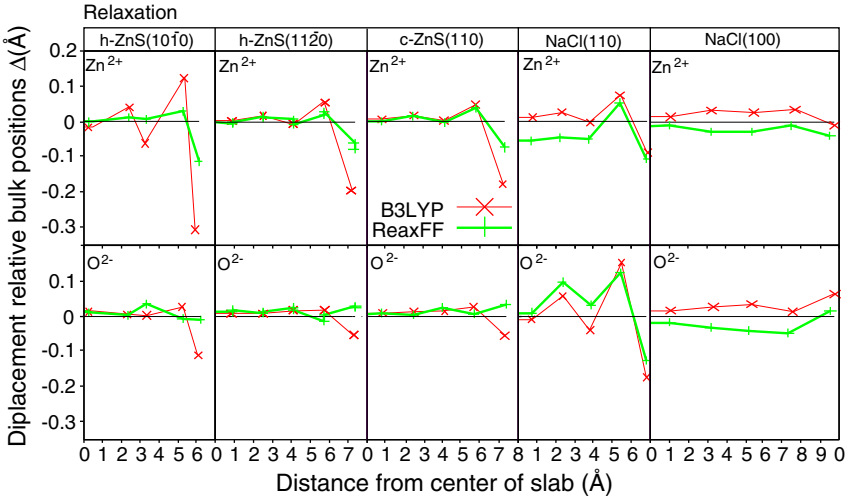

Fig. 3. Atomic displacements (in Å) from the bulk-terminated positions in ZnO slabs as a function of depth (going from the middle to the surface), calculated with the B3LYP and ReaxFF methods.

Table 8
Mulliken charges (B3LYP) and EEM charges (ReaxFF) for bulk ZnO (see text for details)

		B3LYP	ReaxFF
Wurtzite(B4)	Zn	1.026	1.0464
	O	−1.026	−1.0464
Zincblende(B1)	Zn	1.013	1.0402
	O	−1.013	−1.0402
Rocksalt(B3)	Zn	1.095	1.0504
	O	−1.095	−1.0504
CsCl(B2)	Zn	0.978	0.9187
	O	−0.978	−0.9187

QM calculations for the $Zn(OH)_2$ cluster. The ground state was determined through full geometry optimization of the singlet state; this optimized structure was later used as a reference. Subsequently, the total potential energy dissociation profile was constructed through calculations at modified geometries by changing the bond length, allowing other structural parameters to relax, to avoid influence of other straining forces (possibly different in the QM and ReaxFF cases, respectively) on the potential energy curve. The dissociation curve was calculated for both the singlet and triplet states. Finally, the total potential energy of the fully optimized reference structure was subtracted to obtain the interaction energy profile. The QM and ReaxFF curves are shown in Fig. 5a. To the best of our knowledge experimental data such as bond lengths, bond strengths and valence angles for these gas-phase species do not exist, and are therefore not presented in a table for comparison.

To include cluster data for the valence angles, two different clusters were used: $Zn(OH)_2$ and $O(ZnOH)_2$. Explicit cluster data for three out of the four different valence angles (H–O–Zn, O–Zn–O and Zn–O–Zn included) was added. Cluster data for the O–Zn–Zn angle was not added because of the difficulty in getting good quality QM-data for a small cluster with a O–Zn–Zn bond sequence. Following the same procedure as for the bond dissociation profile, the different clusters were relaxed through geometry

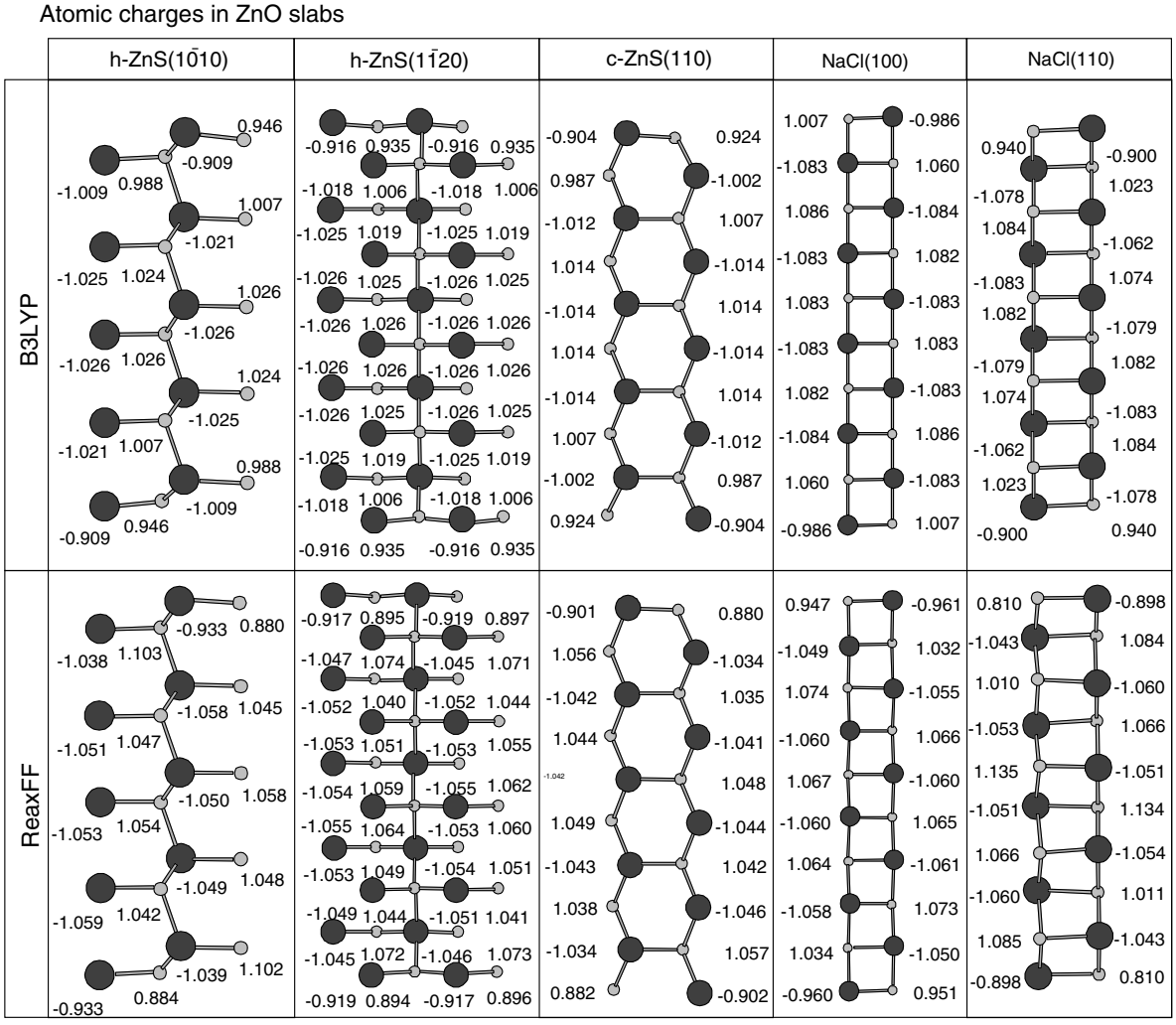

Fig. 4. Atomic charges as a function of depth in the various ZnO slabs. Mulliken charges from B3LYP and EEM-charges from ReaxFF. The surfaces are located at the top and bottom of each figure.

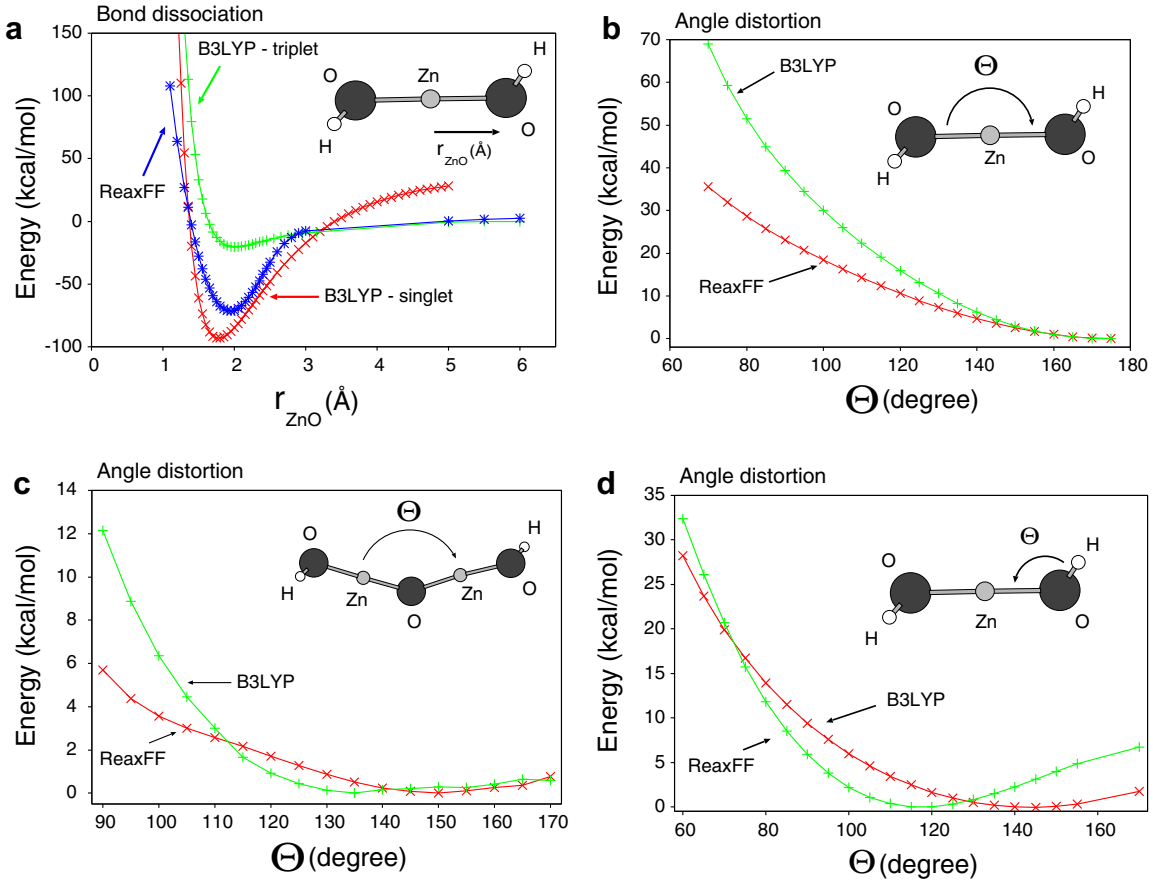

Fig. 5. B3LYP and ReaxFF potential energy curves for: (a) dissociation of a Zn–O bond in the $Zn(OH)_2$ molecule, (b) angle distortion of O–Zn–O in the $Zn(OH)_2$ molecule, (c) angle distortion of Zn–O–Zn in the $O(ZnOH)_2$ molecule, (d) angle distortion of Zn–O–H in the $Zn(OH)_2$ molecule.

optimization, creating two reference states. Afterwards the interesting valence angle (see Fig. 5b–d) was locked in increments, while the other structural parameters were optimized, again to avoid other straining forces in the cluster. This procedure was repeated for each of the two valence angles in the $Zn(OH)_2$ cluster. The resulting potential energy curves are shown in Fig. 5b–d.

In Fig. 5a, it is visible that the crystals in general were prioritized over the clusters since the agreement between the ReaxFF and the B3LYP minima for $Zn(OH)_2$ in Fig. 5a is not perfect. In fact, the ReaxFF minimum is shifted towards 2 Å, which is the equilibrium bond length in the wurtzite and zincblende crystals. Also the depth of the ReaxFF potential well in Fig. 5a is seen to be too shallow, in order to improve (reduce the overestimation of) the heat of formation for ZnO(s) (cf. Fig. 1).

3.5. Errors in the fitted force field

We would like to add a comment concerning the errors in our fitted force field parameters. It is not straightforward to try to assess the quality of the fit by quoting an average or maximum error for the quantities used as observables in the fit. One reason for this is that weighted data points were used in the fitting procedure, and the weighted error will depend on the weighting scheme. The weighting scheme was designed to make sure that the features of the quantum-mechanical data that we considered to be the most important were best reproduced by our fitted FF. Among such features are, as mentioned, the curvature of the volume–energy relationship close to the equilibrium for Wurtzite ZnO, and the order of stability of the various ZnO phases and surfaces. Less emphasis was deliberately put on the gas-phase species, and that is where we consider that the force field has the largest errors.

During the course of the fitting we have used several initial values for the parameters and several weighting schemes. The "final parameters" represent a local minimum for the final weighting scheme and produces the ZnO properties presented in the paper.

4. Application: MD simulation of bulk and surfaces of wurtzite ZnO

In this section we test our new ZnO force field by applying it in two different types of simulation, namely one non-reactive and one reactive. We calculate vibrational mean square amplitudes for the atoms in bulk ZnO and compare them to experimental values from neutron and X-ray

diffraction, to evaluate the ability of ReaxFF to reproduce bulk vibrational properties as a function of temperature. Moreover, we apply our new force-field in studies of crystal growth on the wurtzite ZnO(0 0 0 1) surface, following the procedure of Kubo et al. [15].

4.1. Vibrational mean square amplitudes for bulk ZnO

In all simulations, the equations of motion were solved with the Verlet algorithm, using a time step of 0.25 fs. The temperature was kept constant using the Berendsen thermostat [41]. The volume of the box was equilibrated using the NPT (constant temperature/constant pressure) MD method, where the Berendsen barostat [41] was used to keep the internal pressure of the box at 0 GPa during the subsequent NVT simulations. The system consisted of 360 ions in a simulation box, initially of the dimensions 16.5 Å × 16.6 Å × 17.2 Å. The system was equilibrated for 200 ps simulation time prior to the production runs where trajectories were recorded during 800 ps.

Fig. 6 shows a comparison between atomic mean square amplitudes from the ReaxFF model and anisotropic temperature coefficients from diffraction experiments. The temperature coefficients give a measure of the average vibrational motion of the ions around their equilibrium positions in the crystal. Neutron data was taken from Albertsson et al. [23] and X-ray data from Schultz and Thiemann [42] and Kihara and Donnay [43]. The numerical values from the ReaxFF model are given in Table 9. We observe good agreement between the ReaxFF model and experimental data.

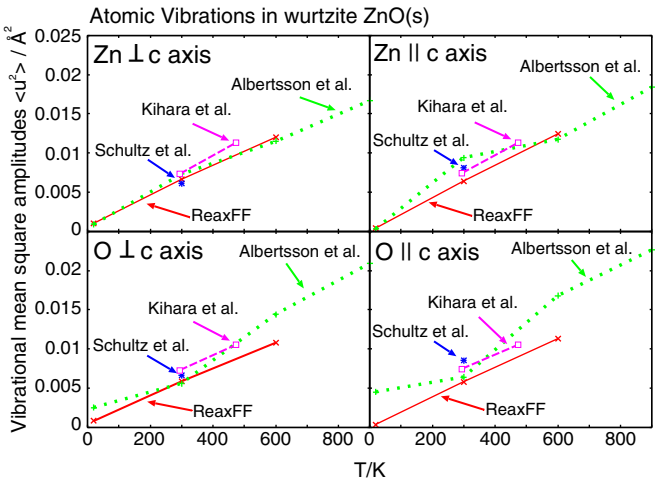

Fig. 6. Atomic vibrational mean square amplitudes for wurtzite ZnO(s). ReaxFF and experimental values from neutron [23] and X-ray diffraction [42,43].

4.2. ZnO surfaces and crystal growth

Here we employed conditions as close as possible to the conditions used in the simulations of ZnO(0 0 0 1) crystal growth by Kubo et al. in Ref. [15]. In this model, the top of the simulation box corresponds to a source which emits ZnO monomer molecules towards a ZnO slab corresponding to a substrate. Two slab models were used under three-dimensional periodic boundary conditions, namely one smooth and one stepped surface. The stepped surface was created by removing half a surface layer on each side of the slab, resulting in two kinks on each side of the slab. The surface area was in both cases 16.45 × 17.10 Å^2, and the thickness approximately 13.8 Å. The vacuum gap separating the oxide slabs was 50 Å. ZnO molecules were made to emerge with random velocities (distributed on a half sphere with radius 900 m/s) from the emitting source located 20 Å above the surface. The molecules were emitted one by one at regular time intervals of 2 ps. The system was equilibrated for 40 ps, prior to the epitaxial growth simulations. The calculations were performed for 30 ps, and a total of 15 ZnO molecules were deposited on the ZnO(0 0 0 1) surface; this corresponds to half a monolayer. The temperature was kept constant at 700 K, which is similar to experimental growth conditions.

In addition to the procedure outlined in Ref. [15], we carried out additionally nine simulations runs for each of the two surface models, to improve the statistics. Moreover, to allow the surfaces to properly relax and reconstruct, the simulations were extended with 300 ps, during which time the number of ions was kept fixed. In all simulations, the equations of motion were solved with the Verlet algorithm using a time step of 0.25 fs. The temperature was kept constant using the Berendsen thermostat [41] and the volume of the box was kept constant.

For both the smooth surface (see Fig. 7) and the stepped surface (see Fig. 8) we see crystal growth. In this respect our model disagrees with the results in Ref. [15], where growth was only observed for the stepped surface. In our simulations of the smooth surface we find no preferential growth position and the incoming dimers distribute them-

Table 9
Atomic vibrational mean square amplitudes in wurtzite ZnO, $\langle u^2 \rangle$, parallel (U_{33}) and perpendicular (U_{11}) to the c axis, calculated from the ReaxFF model at 20 K, 300 K and 600 K

	20 K		300 K		600 K	
	$\perp$ c axis	$\parallel$ c axis	$\perp$ c axis	$\parallel$ c axis	$\perp$ c axis	$\parallel$ c axis
$\langle u^2 \rangle_{Zn}/(Å^2)$	0.00098(8)	0.00041(2)	0.0066(0)	0.0064(2)	0.0120(2)	0.0124(2)
$\langle u^2 \rangle_{O}/(Å^2)$	0.00081(7)	0.00036(2)	0.0059(0)	0.0058(1)	0.0108(1)	0.0113(1)

The number in parentheses is the standard error of the mean.

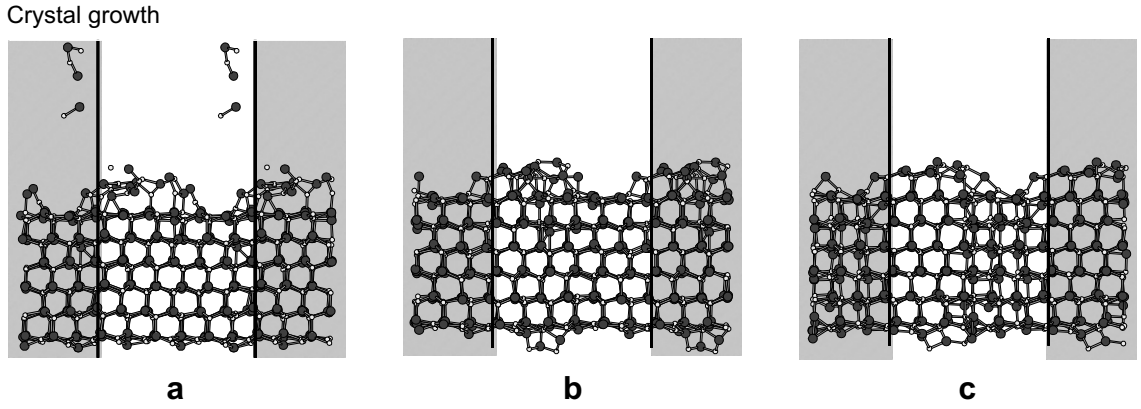

Fig. 7. Snapshots taken from one of the MD simulations of crystal growth on a smooth wurtzite ZnO(0 0 0 1)-surface at 700 K, at (a) 30 ps, (b) 130 ps and (c) 300 ps after the end of equilibration. ZnO molecules were added during the first 30 ps of simulation.

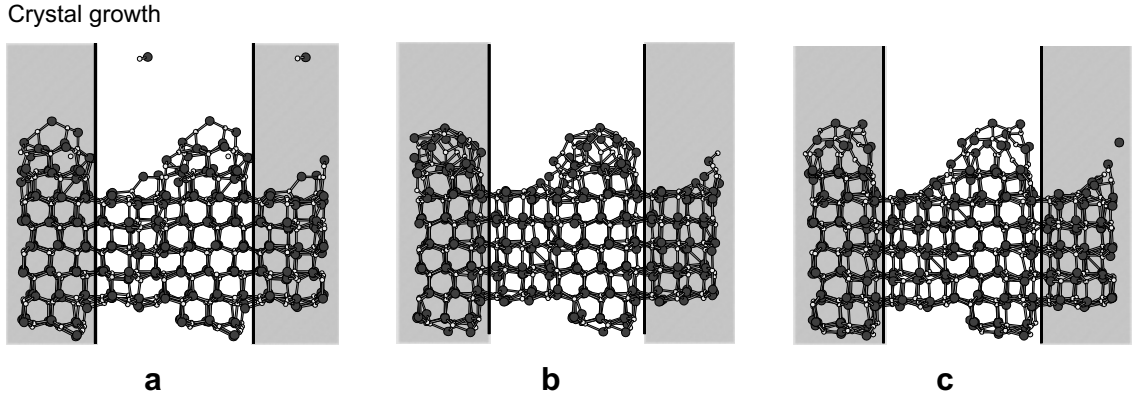

Fig. 8. Snapshots taken from one of the MD simulations of crystal growth on a stepped wurtzite ZnO(0 0 0 1)-surface at 700 K, at (a) 30 ps, (b) 130 ps and (c) 300 ps after the end of equilibration. ZnO molecules were added during the first 30 ps of simulation.

selves randomly over the surface. During the subsequent, extended MD simulation, an increasingly well ordered ZnO(0 0 0 1) layer was formed. We see this behavior in 8 out of the 10 simulation runs.

In simulations of the stepped surface, both Ref. [15] and ourselves find that the molecules preferentially adsorb close to the kinks. We find that the ZnO molecules adsorb both on the upper and the lower sides of the kinks. Our result for the stepped surface is that the growth, rather than mending the broken layer by filling the trench, forms two new facets on either side of the broken layer. We see this behavior in 9 out of the 10 simulation runs. We believe that if the growth had been allowed to continue, these two new facets would eventually meet each other in the trench, and subsequently order into a ZnO(0 0 0 1) monolayer. However, the surface would then be permanently altered towards a stepped surface with terraces of lower surface-energy facets, most probably with large ZnO($1\,0\,\bar{1}\,0$) character. A more rigorous treatment is needed to extract the maximum amount of information from the force field about mechanisms and rates for crystal growth. However, we can already from these simulations conclude that different growth behavior is observed depending on the presence of surface steps.

5. Summary

The present work presents a reactive force field for ZnO, developed to allow an accurate description of the chemical and physical properties of condensed-phase ZnO. Good agreement with DFT calculations is observed for various condensed systems, bulk and surfaces. Emphasis has been put on obtaining a good surface description, to allow future studies of surface chemical reactions important for catalysis. The force field successfully reproduces the atomic vibrational mean square amplitudes of bulk ZnO. Moreover, the force field was used to model crystal growth. We observe a distinct growth pattern dependence on surface structure; on a smooth surface we find a random growth pattern, while a stepped surface causes a distinct growth pattern related to preferential reactions near surface kink-sites. This latter observation is in agreement with earlier simulations on ZnO crystal growth from the literature.

Acknowledgements

This work was supported by the Swedish Research Council (VR). Valuable assistance with the quantum-mechanical bulk calculations was given by Dr. Qing Zhang and Mr. Henrik Eriksson. Many useful discussions with Dr. Pavlin Mitev are acknowledged.

References

[1] Z.R. Tian, J.A. Voigt, J. Liu, B. McKenzie, M.J. McDermott, M.A. Rodriguez, H. Konishi, H. Xu, Nat. Mater. 2 (2003) 821.
[2] G.A. Somorjai, Introduction to Surface Chemistry and Catalysis, John Wiley & Sons, Inc., New York, USA, 1994.
[3] P. Persson, L. Ojamäe, Chem. Phys. Lett. 321 (3–4) (2000) 302.
[4] Ü. Özgür, Y.I. Alivov, C. Liu, M.A.R.A. Teke, S. Dogan, V. Avrutin, S.J. Cho, H. Morkoc, J. Appl. Phys. 98 (2005) 041301.
[5] M. Catti, Y. Noel, R. Dovesi, J. Phys. Chem. Solids 64 (2003) 2183.
[6] J. Serrano, A. Romero, F. Lauck, M. Cardona, A. Rubio, Phys. Rev. B 69 (2004) 094306.
[7] Z.G. Yu, H. Gong, P. Wu, J. Cryst. Growth 287 (2006) 199.
[8] C. Lee, W. Yang, R. Parr, Phys. Rev. B 37 (1988) 785.
[9] A.D. Becke, J. Chem. Phys. 98 (1993) 5968.
[10] B. Dick, A. Overhauser, Phys. Rev. 112 (1958) 90.
[11] D.J. Binks, R.W. Grimes, J. Am. Ceram. Soc. 76 (1993) 2370.
[12] L. Whitmore, A.A. Sokol, C.R.A. Catlow, Surf. Sci. 498 (2001) 135.
[13] A.A. Sokol, S.T. Bromley, S.A. French, C.R.A. Catlow, P. Sherwood, Int. J. Quantum Chem. 99 (2004) 695.
[14] A.J. Kulkarni, M. Zhou, F.J. Ke, Nanotechnology 16 (2005) 2749.
[15] M. Kubo, Y. Oumi, H. Takaba, A. Chatterjee, A. Miyamoto, M. Kawasaki, M. Yoshimoto, H. Koinuma, Phys. Rev. B 61 (23) (2000) 16187.
[16] P. Erhart, N. Juslin, O. Goy, K. Nordlund, R. Müller, K. Albe, J. Phys. Cond. Matter 18 (2006) 6585.
[17] A.C.T. van Duin, S. Dasgupta, F. Lorant, W.A. Goddard III, J. Phys. Chem. A 105 (2001) 9396.
[18] A.C.T. van Duin, A. Strachan, S. Stewman, Q. Zhang, X. Xu, W.A. Goddard III, J. Phys. Chem. A 107 (2003) 3803.
[19] Q. Zhang, T. Cagin, A.C.T. van Duin, W.A. Goddard III, Y. Qi, G. Hector, Phys. Rev. B 69 (2004) 045423.
[20] G.O.A. Janssens, B.G. Baekelandt, H. Toufar, W.J. Martier, R.A. Shoonheydt, J. Phys. Chem. B 99 (1995) 3251.
[21] W.A. Goddard III, A.C.T. van Duin, K. Chenoweth, M. Cheng, S. Pudar, J. Oxgaard, B. Merinov, Y.H. Jang, P. Persson, Topics Catal. 38 (2006) 1.
[22] T. Hahn, International Tables for Crystallography Volume A: Space-group symmetry, IUCr, Chester, UK, 2002.
[23] J. Albertsson, S.C. Abrahams, Å. Kvick, Acta Crystall. B 45 (1) (1989) 34.
[24] J.E. Jaffe, A.C. Hess, Phys. Rev. B 48 (1993) 7903.
[25] A.C.T. van Duin, J.M.A. Baas, B.J. van de Graaf, J. Chem. Soc., Faraday Trans. 90 (1994) 2881.
[26] M.J. Frisch, G.W. Trucks, H.B. Schlegel, G.E. Scuseria, M.A. Robb, J.R. Cheeseman, J.A. Montgomery Jr., T. Vreven, K.N. Kudin, J.C. Burant, J.M. Millam, S.S. Iyengar, J. Tomasi, V. Barone, B. Mennucci, M. Cossi, G. Scalmani, N. Rega, G.A. Petersson, H. Nakatsuji, M. Hada, M. Ehara, K. Toyota, R. Fukuda, J. Hasegawa, M. Ishida, T. Nakajima, Y. Honda, O. Kitao, H. Nakai, M. Klene, X. Li, J.E. Knox, H.P. Hratchian, J.B. Cross, V. Bakken, C. Adamo, J. Jaramillo, R. Gomperts, R.E. Stratmann, O. Yazyev, A.J. Austin, R. Cammi, C. Pomelli, J.W. Ochterski, P.Y. Ayala, K. Morokuma, G.A. Voth, P. Salvador, J.J. Dannenberg, V.G. Zakrzewski, S. Dapprich, A.D. Daniels, M.C. Strain, O. Farkas, D.K. Malick, A.D. Rabuck, K. Raghavachari, J.B. Foresman, J.V. Ortiz, Q. Cui, A.G. Baboul, S. Clifford, J. Cioslowski, B.B. Stefanov, G. Liu, A. Liashenko, P. Piskorz, I. Komaromi, R.L. Martin, D.J. Fox, T. Keith, M.A. Al-Laham, C.Y. Peng, A. Nanayakkara, M. Challacombe, P.M.W. Gill, B. Johnson, W. Chen, M.W. Wong, C. Gonzalez, J.A. Pople, Gaussian 03, Revision C.02, Gaussian, Inc., Wallingford, CT, 2004.
[27] V.R. Saunders, R. Dovesi, C. Roetti, R. Orlando, C.M. Zicovich-Wilson, N. Harrison, K. Doll, B. Civalleri, I. Bush, P.D. Arco, M. Llunell, CRYSTAL2003 User's Manual (2003).
[28] P.J. Schultz, A description of the method is in P.J. Feibelman, Phys. Rev. B 35 (1987) 2626.
[29] L. Fast, J. Wills, B. Johansson, O. Eriksson, J. Inst. Metals 83 (1995) 49.
[30] A. Wander, N. Harrison, Surf. Sci. 457 (2000) 342.
[31] J. Jaffe, A. Hess, J. Chem. Phys. 104 (1996) 3348.
[32] Y. Noel, C.M. Zicovich-Wilson, B. Civalleri, P. D'Arco, R. Dovesi, Phys. Rev. B 65 (2001) 014111.
[33] H. Monkhorst, J. Pack, Phys. Rev. B 13 (1976) 5188.
[34] J. Perdew, K. Burke, M. Ernzehof, Phys. Rev. Lett. 77 (1996) 3865.
[35] M. Fuchs, M. Scheffler, Comput. Phys. Commun. 119 (1999) 67.
[36] G. Aylward, T. Findlay, S.I. Chemical Data, John Wiley & Sons, Ltd., Milton, Australia, 1987.
[37] W.L. Masterton, E.J. Slowinski, C.L. Stanitski, Chemical Principles, CBS, New York, USA, 1987.
[38] R. Krishnan, J.S. Binkley, R. Seeger, J.A. Pople, J. Chem. Phys. 72 (1980) 650.
[39] T. Clark, J. Chandrasekhar, G.W. Spitznagel, P.v.R. Schleyer, J. Comp. Chem. 4 (1983) 294.
[40] K. Raghavachari, G.W. Trucks, J. Chem. Phys. 91 (1989) 1062.
[41] H.J.C. Berendsen, J.P.M. Postma, W.F.V. Gunsteren, A. DiNola, J.R. Haak, J. Chem. Phys. 81 (1984) 3684.
[42] H. Schultz, K.H. Thiemann, Solid State Commun. 32 (1979) 783.
[43] K. Kihara, G. Donnay, Can. Miner. 23 (1985) 647.
[44] S. Desgreniers, Phys. Rev. B 58 (1998) 14102.
[45] T. Bateman, J. Appl. Phys. 33 (1962) 3309.
[46] W.P.H. Karzel, M. Kofferlein, W. Schiessl, M. Steiner, U. Hiller, G.M. Kalvius, D.W. Mitchell, T.P. Das, P. Blaha, K. Schwarz, M.P. Pasternak, Phys. Rev. B 58 (1998) 14102.
[47] J. Brown, J. Inst. Metals 83 (1955) 49.
[48] H. Ledbetter, J. Phys. Chem. Ref. Data 6 (1977) 1181.
[49] K. Chenoweth, A.C.T. van Duin, W.A. Goddard III, J. Phys. Chem. A. (2008), doi:10.1021/jp709896w.